JOURNAL OF MATERIALS SCIENCE **36** (2001) 3539–3547

High creep exponents in a nearly-lamellar γ-based titanium aluminide intermetallic

S. M. ALLAMEH
The Princeton Materials Institute and The Department of Mechanical and Aerospace Engineering, Princeton University, Princeton, NJ 08544, USA

Y. LI
Department of Materials Science and Engineering, The Ohio State University, Columbus, OH 43210, USA

R. J. LEDERICH
The Boeing Company, P. O. Box 516, St. Louis, MO 63166, USA

W. O. SOBOYEJO
The Princeton Materials Institute and The Department of Mechanical and Aerospace Engineering, Princeton University, Princeton, NJ 08544, USA
E-mail: soboyejo@princeton.edu

Secondary creep data are reported for an extruded nearly-lamellar Ti-48Al-1.5Cr-alloy tested in a temperature range of 700 to 900°C. Within this temperature regime, this alloy exhibits a two-stage creep deformation behavior, with relatively high (approximately 8–12) creep exponents occurring in the high stress/high temperature regime. The high exponents in this regime are explained by dynamic recrystallization phenomena observed $\alpha_2 + \gamma$ in the nearly-lamellar microstructure.

1. Introduction

Gamma-titanium-based alloys with a lamellar- or near-lamellar microstructure have been shown to have improved fracture toughness [1–3] and fatigue crack growth resistance [4–7] compared with those of duplex $\alpha_2 + \gamma$ alloys with equiaxed microstructures. Lamellar gamma alloys have also been shown to have better creep resistance than alloys with equiaxed micrstructures [8–11]. However, prior studies of secondary creep deformation in lamellar and equiaxed gamma alloys suggest that the secondary creep exponents may be anomalously high in some microstructural/alloying conditions [11–17].

In the case of Ti-48Al-1.5Cr and Ti-48Al-2Cr-2Nb, the high creep exponents (between 8 and 14) were attributed originally to the effects of constant structure creep [11]. It will be shown in this paper, that the results of transmission electron microscopy analyses of crept Ti-48Al-1.5Cr specimens do not support the possibility of constant structure creep in this alloy. Instead, the microstructural analysis reveals the occurrence of dynamic recrystallization phenomena in the nearly-lamellar microstructures. Since the dynamic recrystallization reduces the effective grain size during creep deformation, it is suggested that the apparently high creep exponents are due largely to the faster secondary creep rates associated with smaller overall grain sizes.

2. Materials

The γ-based titanium aluminide alloy that was used in this experiment was produced by Flowserve, (formerly Duriron) Inc., Dayton OH, in the form of cylindrical billets of 150 mm diameter. The ingot was then extruded, at Wright Patterson Ai-Force Base, Dayton OH, at 1343 °C with a reduction of 14:1. The chemical composition of the alloy, determined by combustometric techniques, was 49.1% Al, 1.79% Cr, 0.035% C, 0.0103% O, 0.011% N, 0.075% H and a balance of Ti (compositions quoted in atomic %). Tensile specimens, with an average gage diameter of 6 mm and an average gage length of 25 mm were fabricated by electro-discharge machining (EDM), followed by turning into cylindrical shape.

The specimens were heat treated according to the empirical schedule shown in Fig. 1. This included: an initial heat treatment at 982°C for 4 h and air-cooling; heat treatment at 815°C for 24 h and furnace cooling, and heat treatment at 815°C for 24 h followed by air cooling. This empirical heat treatment profile, designated as HTC in previous work [3], was chosen because it yields a very good balance of room-temperature and elevated-temperature properties, according to several studies of mechanical properties of γ-titanium alloys produced by both powder metallurgy [3] and ingot metallurgy [18] techniques.

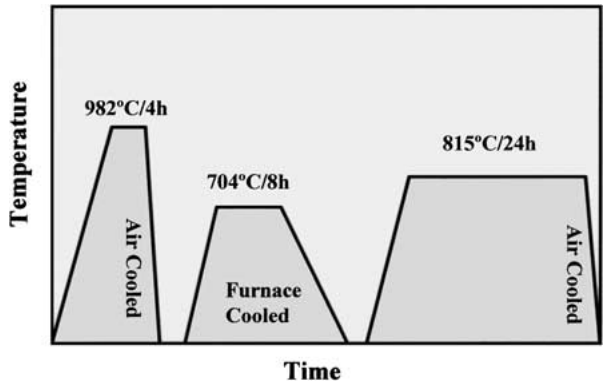

Figure 1 Time-temperature profile for heat treatment (HTC) of the ternary Ti-48Al-1.5Cr alloy.

The nearly lamellar microstructures of the undeformed and deformed heat-treated material are shown in Fig. 2a and b, respectively. The heat-treated microstructure consists of partially recrystallized coarse grains (about 200 μm average colony size) prior to deformation (Fig. 2a). This microstructure (Fig. 2a) undergoes further recrystallization during creep deformation (Fig. 2b). Finer equiaxed grains (5–15 μm average size) develop during creep deformation, especially at the prior gamma grain boundaries and triple points (Fig. 2b).

Coarsening and limited bowing of laths (Fig. 2b) were observed after creep deformation at 900°C for 20 h. A thick (200 μm thick) oxide layer was also observed on the surfaces of the deformed specimens. Transmission electron microscopy (TEM) analysis of the undeformed samples revealed a recovered microstructure with relatively low dislocation density, as shown in Fig. 3. This TEM micrograph also shows the lath morphologies in the initially straight nearly-lamellar microstructure. The average width of the γ lamellae was approximately 400 nm while the average width of the α_2 lamellae was about 200 nm.

A summary of the tensile properties of the heat-treated Ti-48Al-1.5Cr alloy is presented in Table I for comparison with the creep loading conditions. All high temperature tensile tests were carried out at constant strain rate of 5×10^{-4} s^{-1}. The 0.2% offset yield strength decreases from 607 MPa, at room temperature, to 704 MPa at 815°C. The corresponding change in the ultimate tensile strength is a decrease from 704 to 659 MPa. The plastic elongation to failure also increases from 1.4% to 25.6%, as the temperature is increased from 25 to 815°C.

TABLE I A summary of the tensile properties of Ti-48Al-1.5Cr at room-and elevated temperature

Tensile properties	Room temperature	Elevated temperature (815°C)
0.2% off set yield strength (MPa)	607	555
Ultimate tnesile strength (MPa)	704	659
Young's Modulus (GPa)	160	—
Elongation to Failure (%)	1.4	25.6

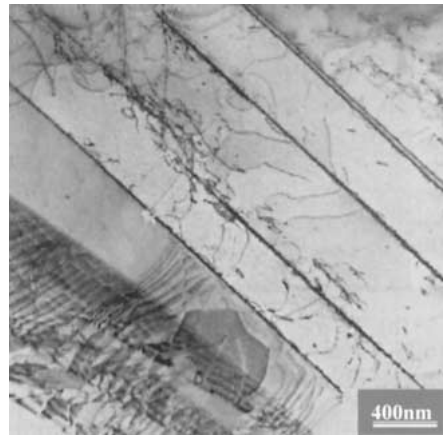

Figure 3 TEM image of undeformed section of the Ti-48Al-1.5Cr specimen.

3. Experimental procedures

Tensile creep tests were performed on similar specimens to those employed in the tensile tests. The experiments were conducted in air at temperatures of 700, 800 and 900°C. The initial mean stresses ranged from 70 to 400 MPa, and creep rates were determined at 3–6 different stress levels for each temperature regime. Displacements during creep were monitored using a linear voltage displacement transducer (LVDT) attached to gage sections.

Creep testing was continued until steady-state creep conditions were established for a minimum of 24 h. For most specimens, and for each temperature, the mean stresses were increased in increments of approximately 100 MPa, and the above procedure was repeated until new steady-state conditions were established. This

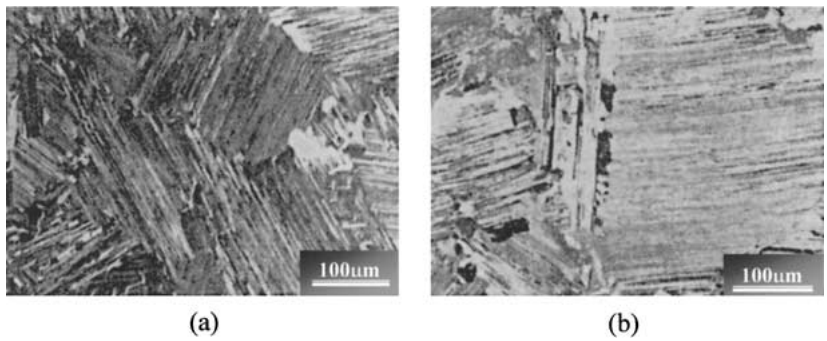

Figure 2 Nearly-lamellar Microstructure of Ti-48Al-1.5Cr alloy after the HTC anneal (a) Before deformation and (b) After deformation.

made it possible to obtain steady-state creep data for multiple stress levels at the same temperature.

In contrast to specimens subjected to multiple stress levels, some specimens were tested only under one stress level, making it possible to evaluate the effect of multiple stress levels on creep behavior. In general, good agreement was observed between the secondary rate data obtained from specimens subjected to a single stress level, and those deformed at multiple stress levels.

Transmission electron microscopy analysis was carried out on thin foils extracted from the gage sections of the specimens that were deformed only at a single stress level. The foils, which were extracted via electro-discharge machining, were electro-polished in a perchloric acid solution. They were then examined in a transmission electron microscope (TEM) operated at 200 kV. TEM was used to examine the microstructure of foils prepared from both deformed and undeformed sections of the specimens subjected to creep deformation. This made it possible to distinguish between the substructures due to creep, and those that occurred primarily as a result of thermally-induced phase transformations.

The thinned sections of the TEM foils of the deformed gage sections were also studied using an optical microscope equipped with a polarizer and a high-intensity xenon light source. This microscope made it possible to examine the evidence of dynamic recrystallization without etching. For comparison, metallographic cross sections of selected specimens were also examined after grinding and diamond polishing with standard techniques.

4. Results and discussion

4.1. Secondary creep rates

A plot of the secondary creep rate versus applied initial stress is presented for the Ti-48Al-1.5Cr alloy in Fig. 4. There are two distinct (stress-temperature) regimes associated with secondary creep behavior. In the low stress regime, (80–400 MPa) the secondary creep exponents are 2.4, 2.3 and 3.5 at 700, 800 and 900°C. However, in the high stress regime (>400 MPa), the corresponding stress exponents for the same temperatures are 14.3, 12.0 and 8.6.

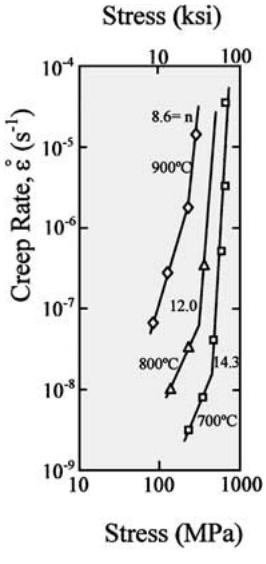

Figure 4 Secondary creep rate data for the Ti-48Al-1.5Cr.

The steady-state creep activation energy for a mean stress of 200 MPa was determined to be 292 kJ/mol. This value is close to that of self-diffusion of Ti in single phase γ-TiAl (290 kJ/mol) and is also close to 300 kJ/mol reported by Ref. [34] and suggests a dislocation climb dislocation mechanism could be operational. This is typical for the lower creep exponent regime as evidenced by values of 300 kJ/mol reported by Martin *et al*. [30] for a Ti-50.3 Al made by powder metallurgy, and hot extruded at 1413°C. The microstructure was lamellar $+\gamma$ colony, and the alloy was tested at 103–241 MPa in the temperature range of 700–950°C. This resulted in a creep exponent of 4.

A higher activation energy was reported by Hayes and London [9] (320–341 kJ/mol) for Ti-48Al-1Nb with a lamellar "colonies + equiaxed" γ structure tested at 704–850°C under 103–241 MPa stress with a creep exponent of 4.5–5. Higher activation energies are associated with higher creep exponents.

An activation energy of 359 kJ/mol was reported by Takahashi and Oikawa for a Ti-50Al in as-cast condition with "lamellar $+\gamma$ colony boundaries" structure tested in the stress range of 100–251 MPa. The alloy was tested at 677–877°C and resulted in a high creep exponent of 7.9. A high activation energy of 600 kJ/mol was reported by Oikawa [33] for a Ti-50Al alloy with equiaxed γ grains. This alloy was tested in the stress range of 100–400 MPa at 827 °C, resulting in a high exponent of 7.7.

For Ti-48Al-2Cr-2Nb produced by vacuum arc melting with a duplex microstructure tested at 103–300 MPa, Wheeler *et al*. [31] reported 300 kJ/mol for low stress regime (creep exponent of 3) and 410 kJ/mol for high stress regime (creep exponent of 4). While some of these studies [9, 31, 32] suggest a well-defined steady-state creep, others agree on a minimum creep range [28–30]. The steady-state activation energy associated with the higher-exponent regime was found, in this study, to be 630 kJ/mol at 400 MPa (Fig. 4). The significant differences between the activation energies and the creep exponents suggest that the creep deformation mechanisms are different at the lower and higher strees levels.

The secondary creep exponents of 2.3–3.5 are consistent with dislocation-glide controlled creep [13]. However, the higher exponents of 8.6, 12.0 and 14.3, obtained at higher stress levels are between two and three times greater than those associated with conventional dislocation glide/climb-controlled creep [13]. This indicates that mechanisms other than conventional dislocation-controlled creep, may be operational at the higher strees levels.

4.2. Deformation substructures

The results of TEM on the Ti-48Al-1.5Cr alloy are shown in Fig. 5a and b. The dislocation density in the sample that was tested at 700°C and 220 MPa was

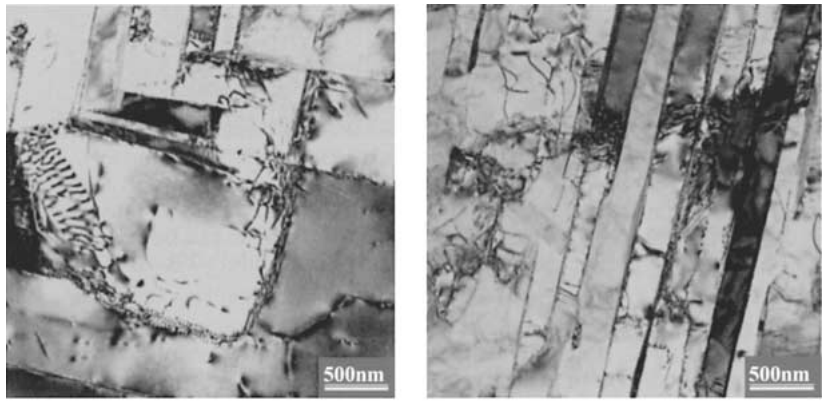

Figure 5 Bright field TEM images from specimens crept at 700°C at stress levels of (a) 220 MPa and (b) at 345 MPa.

relatively low in the deformed section (Fig. 5a), and was comparable to that in the undeformed section (Fig. 3). However, there is a significant increase in dislocation activity at higher stress levels (Fig. 5b). The dislocation configurations at higher stress levels included tangled dislocation networks and hard slip modes (slip across the width of lamellae), as shown in Fig. 5b for a sample deformed at 700°C and 345 MPa. Most of the dislocations observed in this sample were of the 1/2 [110] type.

Typical dislocation substructures observed in the sample deformed at 800°C and 220 MPa are presented in Fig. 6a. This shows clear evidence of a soft slip mode (slip along the length the length of the lamellae) and dislocation loops emanating from lamellar boundaries. The relative contributions of these dislocation loops to the creep deformation are not well understood at this time. In the higher stress regimes, at 800°C, the dislocation density is increased significantly and some of the lamellae are bowed as a result of the deformation.

The substructures observed in the specimens tested at 900°C at a mean stress of 86 MPa (low stress regime), reveal clear evidence of a tangled dislocation network (Fig. 7a). This dislocation network is the reminiscent of

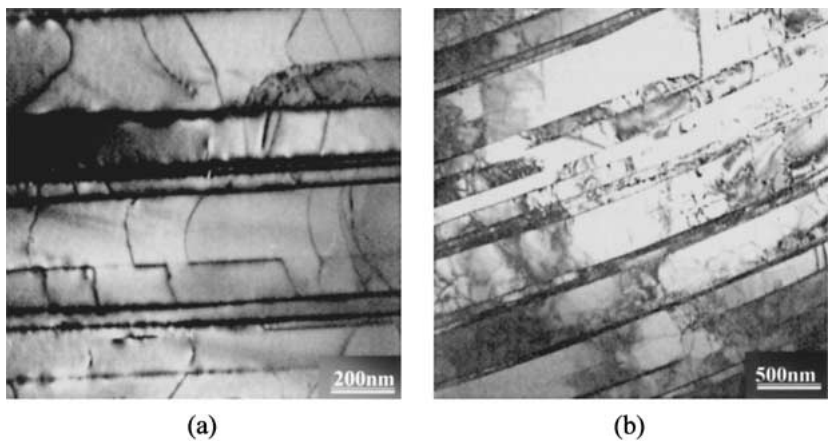

Figure 6 Bright field TEM images of specimens deformed at 900°C under stress levels of (a) 220 MPa and (b) 345 MPa.

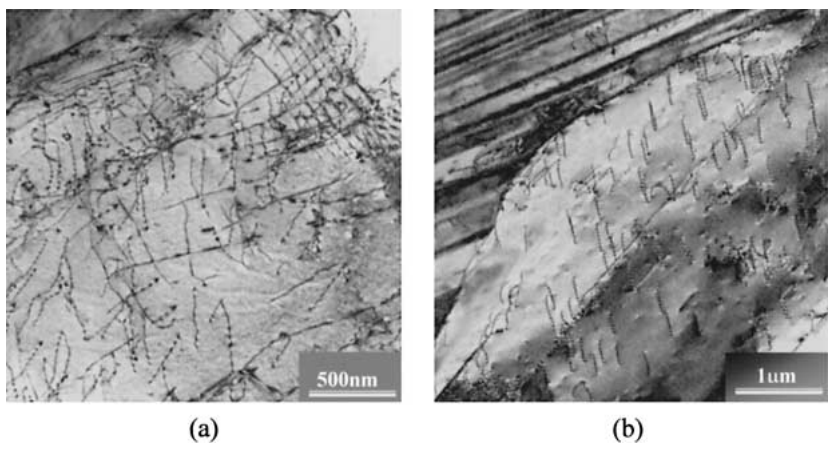

Figure 7 Bright field TEM images of specimens deformed at 900°C under stress levels of (A) 86 MPa, and (b) 138 MPa.

the earliest stages of a cell structure. In contrast, samples tested at the same temperature, but under a mean stress of 138 MPa (higher stress regime), exhibit a high-density of individual dislocations within a "staircase" arrangement (Fig. 7b).

4.3. Dynamic recrystallization

TEM foils extracted from the deformed sections of the crept specimens were studied in an optical microscope under polarized light from a xenon high-intensity light source. The polarized light imaging revealed strong evidence of dynamic recrystallization, as shown in Fig. 8a–d. Furthermore, as the test temperature or stress level is increased, the extent of dynamic recrystallization was observed to increase. However, this increase was less pronounced for increased stress than it was for increased temperature.

To quantify the extent of dynamic recrystallization, qualitative image analyses of the photomicrographs (Fig. 8a–d) was carried out. The results are summarized in Fig. 9. This shows a plot of the volume fraction of dynamically recrystallized grains against mean stress, for temperatures between 700 and 900°C. It is important to note here that the volume fraction of recrystallized grains was calculated by subtracting the volume fraction of the recrystallized grains before creep deformation from the total volume of recrystallized grains after creep deformation. Similar evidence of dynamic recrystallization has been observed in gamma alloys by numerous research groups [12, 23–27].

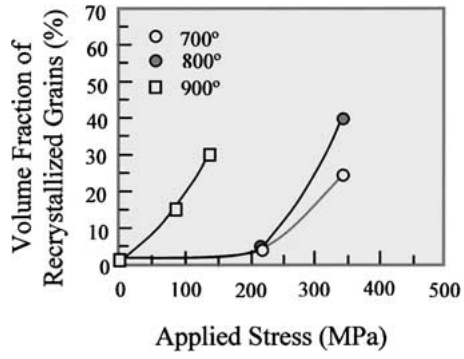

Figure 9 Volume fraction of recrystallized grains plotted for various temperatures as a function of applied stress.

4.4. Related prior work

Significant efforts have been made by a number of researchers to study the creep deformation mechanisms in gamma-based alloys [9–17, 20–22]. All of these studies

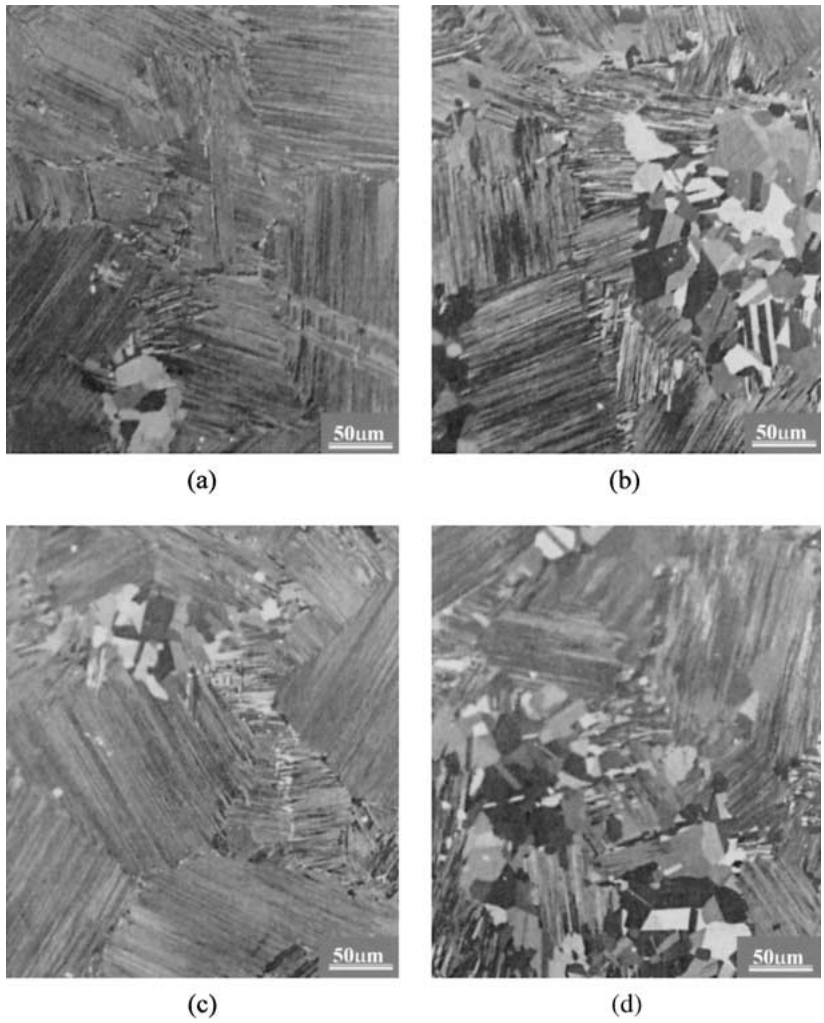

Figure 8 Evidence of dynamically recrystallized grains in specimens deformed at (a) 700°C/220 MPa, (b) 700°C/345 MPa, (c) 800°C/220 MPa and (d) 900°C/138 MPa.

conclude that creep is dislocation-controlled, especially at higher stresses (greater than ∼200–300 MPa). However, relatively low secondary creep exponents (between 1 and 2) have also been reported at low stresses (below ∼200 MPa) [11, 14, 17], suggesting a possible role of diffusion-controlled creep mechanisms [11, 14] in this regime. Lower activation energies (approximately half of those in the high stress regime) and secondary creep exponents close to 2 have also been suggested as evidence of Coble creep in some alloys [11, 17]. However, these have not been corroborated with experimental evidence from scratch/grid displacement experiments.

At stresses above ∼300 MPa, a number of mechanisms have been associated with creep deformation in gamma alloys. As stated earlier, all the studies acknowledge the significant role of dislocation-controlled creep [9–18, 20–22], which is generally expected when the secondary creep exponent is between 3 and 7. However, a number of researchers [11, 14, 16, 17] have reported higher creep exponents between 7 and 14. Soboyejo *et al*. [11] and Wang [17] attributed this to the possible effects of constant structure creep which tends to give the squared stress, $(\sigma^2)^n$ dependence that gives rise to creep exponents that can very between 7 and 14 [11, 17]. Such dependence can be written as: $\dot{\varepsilon} = A(\frac{\sigma^2}{d})^{2n} \exp(\frac{-Q}{RT})$ which shows an apparent exponent twice that of a conventional creep exponent. However, the TEM analyses in this study do not support this argument.

In addition to conventional dislocation-controlled creep, other researchers [12, 22] have also demonstrated that significant levels of deformation-induced twinning can occur in some gamma alloys. Since the formation of deformation twins involves the movement of [112]-type partial dislocations, and the formation of complex stacking faults, this may be considered as a special case of dislocation-controlled creep. Furthermore, deformation – induced twinning has not been shown to always give rise to higher creep exponents, although Skrotzki's result [12] of $n = 8$ is somewhat higher than what would be expected for dislocation-controlled creep [19].

Another factor that can contribute to creep deformation behavior at higher stresses is the fact that dislocations are emitted from the interfaces between lamellae during creep deformation [15, 20]. Such interfacial dislocations may give rise to faster creep rates by increasing the population of mobile dislocations. However, they may also assist with the accommodation of grain boundary deformation. The role of interfacial dislocations in the elevation of the stress exponents is, therefore, unclear.

4.5. The source of apparently high creep exponents

The phenomenological equation that has been used to characterize secondary creep rate, $\dot{\varepsilon}_s$, is generally of the form [19]:

$$\dot{\varepsilon}_s \frac{A}{d^m}(\sigma)^n \exp\left(-\frac{Q}{RT}\right) \tag{1}$$

where A is a material mechanism constant, m is generally equal to 2 except for the case of grain boundary diffusion-controlled creep for which m is 3, σ is the applied mean stress, d is the grain size, Q is the activation energy, R is the universal gas constant and T is the absolute temperature. In cases where the grain size is constant during creep deformation, taking logarithms of either side of Equation 1 gives:

$$\ln(\dot{\varepsilon}_s) = n \ln \sigma + \ln\left(\frac{A}{d^2}\right) - \frac{Q}{RT} \tag{2}$$

For a constant temperature and a stable microstructure during secondary creep, $\ln(\frac{A}{d^2}) - \frac{Q}{RT}$ is a constant, C_1, which would correspond to the intercept on the $\ln(\dot{\varepsilon}_s)$ axis on a plot of $\ln(\dot{\varepsilon}_s)$ versus $\ln \sigma$. Hence Equation 2 reduces to:

$$\ln(\dot{\varepsilon}_s) = n \ln \sigma + C_1 \tag{3}$$

If the effective grain size, d, decreases due to dynamic recrystallization during creep deformation, then, the intercept on the $\ln(\dot{\varepsilon}_s)$ axis will shift, giving rise to a family of lines with the same slope, n, as the original line. This is shown schematically in Fig. 10a, in which the dashed lines correspond to a family of lines of constant slope, n. The solid line in this figure corresponds to a schematic dependence of $\ln(\dot{\varepsilon}_s)$ on $\ln \sigma$. Note that,

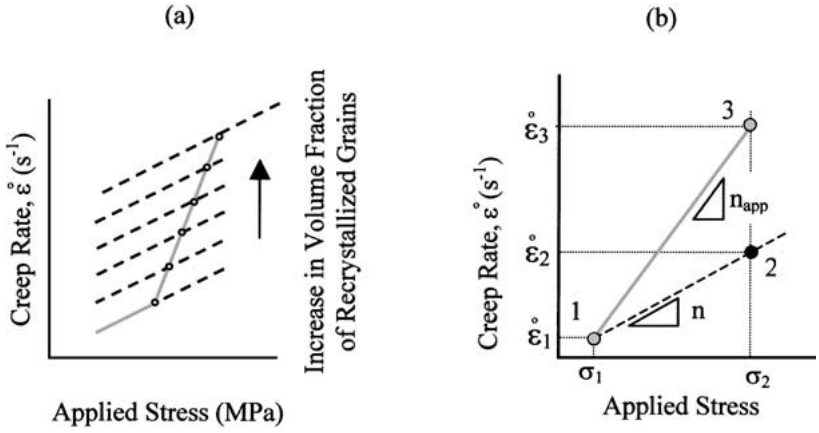

Figure 10 Schematic illustration of the possible effects of dynamic recrystallization on secondary creep rate: (a) The effect of increased volume fraction of recrystallized grains on overall secondary creep rates and creep exponents, and (b) Change in stress exponent due to change in grain size.

for each value of σ, the value of $\dot{\varepsilon}_s$ is increased from the original line by an amount corresponding to the decrease in the effective grain size due to the dynamic recrystallization that occurs during creep deformation.

4.6. Quantifying the increase in the stress exponent

The increase in the stress exponent due to dynamic recrystallization is illustrated in Fig. 10b. It has also been modeled in Appendix A. The model predicts that Δn is given by:

$$\Delta n = n_{app} - n = \frac{2\ln\left(\frac{d_1}{d_2}\right)}{\ln\left(\frac{\sigma_2}{\sigma_1}\right)} \tag{4}$$

It also predicts an increase in the creep exponent if both the stress and the grain size change. From the micrographs showing evidence of dynamic recrystallization, d_1/d_2 is between 2 and 4 for σ_2/σ_1 ratio of 1.5. Substituting these ratios in the Equation (4) gives a Δn value of 3.4 to 6.8.

Since the TEM revealed clear evidence of dislocation creep, classical creep theory suggests that the creep exponent, n, should be between 3 and 7 [19]. However, due to possible dynamic recrystallization phenomena, the apparent stress exponents, $n_{app} = n + \Delta n$, are ~6.4 (3 + 3.4) and 13.8 (7 + 6.8). This is consistent with the range of creep exponents (8.6–14.3) determined from experiments conducted in this study.

However, it is important to note here that, the above model provides only a semi-quantitative rationale for the observed increase in stress exponents. This is partly because it considers only an average grain/colony size in a system that has a predominantly lamellar structure. This is clearly a difficult approximation that must be made in the absence of a better measure of a microstructural unit size for a complex lamellar + equiaxed $\alpha_2 + \gamma$ structure. Furthermore, the model does not account for the degree of recrystallization, except through its influence on the measured grain size.

Nevertheless, the model provides some valuable insights and reasonable semi-quantitative estimates of the possible role that dynamic recrystallization plays in increasing the creep exponents in gamma-based alloys. The predicted apparent creep exponents are also in good agreement with the experimental results.

4.7. Implications

The high secondary creep exponents (Fig. 4) observed for the lamellar Ti-48Al-1.5Cr alloy can, therefore, be attributed to the dynamic recrystallization phenomena (Figs 4 and 8) that occur during creep deformation at higher stresses and temperatures (Fig. 8).

Since dynamic recrystallization reduces the effective grain size during creep deformation, the secondary creep rates, which are generally inversely proportional to the square of grain size, will be faster than those in alloys with stable coarser microstructures, and constant values of d.

Furthermore, as in previous studies [12–18, 20–22], the TEM analyses revealed significant dislocation activity at all the stress levels and temperatures that were examined in this study. However, with the exception of the low stress/low temperature regime, where the extent of dynamic recrystallization was very small, the creep exponents and activation energies appeared to be controlled largely by dynamic recrystallization (Figs 4 and 8).

The above evidence of dynamic recrystallization is consistent with recently published evidence of dynamic recrystallization by numerous research groups [12, 23–28]. These studies show clear evidence of dynamic recrystallization in lamellar gamma alloys, in the so-called primary, secondary, and tertiary creep regimes. This indicates that some lamellar structures may be inherently unstable under creep conditions unless some special efforts are made to stabilize their microstructures via alloying or heat treatment. The improved fatigue crack growth and fracture resistance of lamellar gamma alloys [1–7] may, therefore, be compromised by the effects of dynamic recrystallization.

Furthermore, since the microstructures of some lamellar alloys may be unstable, their mechanical properties may change significantly during creep deformation in the potential service temperature regime (~650–760°C). This may limit some of the potential applications of lamellar gamma alloys in future aeroengines and land-based engines. Further work is clearly needed to develop gamma alloys with microstructures that are resistant to dynamic recrystallization in the potential service temperature range.

5. Conclusions

1. The transmission electron microscopy analyses suggest that creep deformation in the Ti-48Al-1.5Cr alloy involves significant dislocation activity. At lower stresses and temperatures, the creep exponents and activation energies suggest a mechanism of dislocation glide-controlled creep. More complex dislocation configurations (networks and cell structures) are observed at higher stresses and temperatures.

2. The secondary creep behavior at higher stresses is significantly affected by dynamic recrystallization phenomena. The extent of dynamic recrystallization increases with increasing stress and temperature. However, the extent of dynamic recrystallization is more significantly affected by stress, than by temperature. It has the overall effect of reducing the overall grain size of the initial lamellar structure.

3. The high stress exponents at higher stresses and temperatures are attributed to the effects of dynamic recrystallization, which increase with increasing stress and temperature. The possible increase in the creep exponents, due to dynamic recrystallization have also been predicted by a simple model to be in the range between 3.4 and 6.8. These give predictions of apparent stress exponents (6.4–13.8) that are in good agreement with the measured values (8.6–14.3).

Acknowledgements

The research was supported by the Division of Materials Research of the National Science Foundation, with Dr. Bruce MacDonald as the Program Monitor. The authors are grateful to Prof. Ali Argon and Mr. Bob Hayes for useful technical discussions. Appreciation is also extended to Mr. Henk Colijn for assistance with transmission electron microscopy.

Appendix A

Consider three points 1, 2 and 3 in the plot of strain rate against stress shown in Fig. 10b. Point 1 is a regular point on the creep rate-stress curve prior to dynamic recrystallization characterized by σ_1 and $\dot{\bar{\varepsilon}}_1$. Point 2 is located on the curve at an arbitrary creep rate, ε_2, and corresponding stress level, σ_2. However, at this point, the microstructure, and particularly, grain size remain unchanged.

If the microstructure changes, e.g. grain size decreases due to dynamic recrystallization, the resulting creep rate at σ_2, would not be $\dot{\bar{\varepsilon}}_2$, rather, it would be at a higher value, $\dot{\bar{\varepsilon}}_3$, corresponding to point 3. The creep rate [19] for the points 1, 2 and 3 can be expressed as:

$$\ln\left(\dot{\bar{\varepsilon}}_s^1\right) = n\ln\sigma_1 + \ln\left(\frac{A}{d_1^2}\right) - \frac{Q}{RT} \tag{A1}$$

$$\ln\left(\dot{\bar{\varepsilon}}_s^3\right) = n\ln\sigma_2 + \ln\left(\frac{A}{d_2^2}\right) - \frac{Q}{RT} \tag{A2}$$

where d_1 and d_2 denotes the average grains size before and after dynamic recrystallization taking place in the time period lapsed between the two points 1 and 3. It should be noted that $\sigma_2 = \sigma_3$. Hence Equation 2 in the text can be written for these 2 points. Subtracting Equation A1 from Equation A2 gives:

$$\ln\left(\dot{\bar{\varepsilon}}_s^3\right) - \ln\left(\dot{\bar{\varepsilon}}_s^1\right) = n\ln\sigma_3 + \ln\left(\frac{A}{d_2^2}\right) - n\ln\sigma_1 - \ln\left(\frac{A}{d_1^2}\right) \tag{A3}$$

The apparent slope, n_{app} (Fig. 10.b), can also be written as:

$$n_{app} = \frac{\ln\left(\dot{\bar{\varepsilon}}_s^3\right) - \ln\left(\dot{\bar{\varepsilon}}_s^1\right)}{\ln\sigma_3 - \ln\sigma_1} \tag{A4}$$

Substituting Equation A3 into A4, and simplifying gives:

$$n_{app} = \frac{\ln\left(\dot{\bar{\varepsilon}}_s^3\right) - \ln\left(\dot{\bar{\varepsilon}}_s^1\right)}{\ln\sigma_2 - \ln\sigma_1} = \frac{n\ln\sigma_2 - n\ln\sigma_1}{\ln\sigma_2 - \ln\sigma_1} + \frac{\ln\left(\frac{A}{d_2^2}\right) - \ln\left(\frac{A}{d_1^2}\right)}{\ln\sigma_2 - \ln\sigma_1} = n + \frac{2\ln\left(\frac{d_1}{d_2}\right)}{\ln\left(\frac{\sigma_2}{\sigma_1}\right)} \tag{A6}$$

Finally, the increase in the creep exponent, $\Delta n = n_{app} - n$, may be determined by rearranging Equation A5 to give:

$$\Delta n = n_{app} - n = \frac{2\ln\left(\frac{d_1}{d_2}\right)}{\ln\left(\frac{\sigma_2}{\sigma_1}\right)} \tag{A7}$$

References

1. Y. W. KIM and D. M. DIMIDUK, *J. Metals* **43** (1991) 40.
2. K. S. CHAN, *Metall. Trans. A* **24A** (1993) 569.
3. W. O. SOBOYEJO, D. S. SCHWARTZ and S. M. L. SASTRY, *Metall. Trans.* **23A** (1992) 2039.
4. B. D. WORTH, J. M. LARSEN, S. J. BALSONE and J. W. JONES, *ibid.* **28A** (1997) 825.
5. S. J. BALSONE, B. D. WORTH, J. M. LARSEN and J. W. JONES, *Scripta Metall. Mater.* **32** (1995) 1653.
6. J. M. LARSEN, B. D. WORTH, S. J. BALSONE, A. H. ROSENBERGER and J. W. JONES, in "Fatigue '96" (Elsevier Science Ltd., Oxford, UK, 1996) p. 1719.
7. W. O. SOBOYEJO, C. MERCER, K. LOU and S. HEATH, *Metall. Trans.* **26A** (1995) 2275.
8. T. TAKAHASHI, H. NAGAI and H. OIKAWA, *Mater. Sci. Eng.* **A128** (1990) 195.
9. R. W. HAYES and B. LONDON, *Acta Metall. et Mater.* **40** (1992) 2167.
10. M. F. BARTHOLOMEUSZ and J. A. WERT, *Metall. Trans.* **25A** (1994) 2161.
11. W. O. SOBOYEJO and R. J. LEDERICH, "Novel Approaches to the Assessment of Creep Deformation in Gamma-Based Titanium Aluminides," in First Int. Symp. Structural Intermetallics, edited by R. Darolia (TMS, Warrendale, PA, 1993) p. 353.
12. B. SKROTZKI, in Proc. of the 8th Symposium on the Creep and Fracture of Materials, Key Engineering Materials, Vols. 171–174, Trans Tech Publications, Switzerland, 2000) p. 701.
13. Y. G. ZHANG, J. G. LIN and C. Q. CHEN, in Proc. of the 3rd International Workshop on Ordered Intermetallic Alloys and Composites, 5–10 April 1999, China (Transactions of the Nonferrous Metals Society of China, 1999) Vol. 9, Spec. Issue, p. 280.
14. J. BEDDOES, J. TRAINTAFILLIOU and L. ZHAO, in Proc. of High-Temperature Ordered Intermetallic Alloys VII. MRS Fall Meeting, 2–5 Dec. 1996, Boston, MA, Conf. Proc., 1997, p. 293.
15. M. A. MORRIS and M. LEBOEUF, *Intermetallics* **5**(5) (1997) 339.
16. S. SPIGARELLI, L. FRANCESCONI, C. GUARDAMAGNA and E. EVANGELISTA, *Mater. Sci. Eng. A* **A234-23** (1997) 378.
17. J. N. WANG and T. G. NIEH, *Acta Materialia* **46** (1998) 1887.
18. C. MERCER and W. O. SOBOYEJO, in Symp. Fatigue and Fracture of Ordered Intermetallics I, edited by W. O. Soboyejo, T. S. Srivatsan and D. L. Davidson (TMS, Warrendale, PA, 1993) p. 277.
19. T. H. COURTNEY, in "Mechanical Behavior of Materials," (McGraw-Hill, New York, 1990).
20. L. M. HSIUNG and T. G. NIEH, *Mater. Sci. Eng.* **A239–240** (1997) 438.
21. M. LU and K. H. HEMKER, *Acta Materialia* **45** (1997) 3573.
22. Z. JIN and T. R. BIELER, *Phil. Mag. A* **71** (1995) 925.
23. S. L. KAMPE, J. D. BRYANT and L. CHRISTODOULOU, *Metall. Trans. A* **22** (1991) 447.
24. D. A. WHEELER, B. LONDON and D. E. LARSOEN, JR., *Scripta Metall. Mater.* **26** (1992) 939.
25. A. BARTELS, J. SEEGER and H. MECHING, in "High-Temperature Ordered Intermetallic Alloys V," edited by I. Baker, R. Daviola, J. D. Whittenberger and M. H. Yoo (Mater. Res. Soc. Proc. Vol. 288, Pittsburgh, PA, 1993) p. 1179.
26. K. MARUYAMA, T. TAKAHASHI and H. OIKAWA, *Mater. Sci. Eng. A* **153** (1992) 443.
27. O. D. SHERBY, H. K. RODNEY and ALAN K. MILLER, *Metall. Trans. A* **8A** (1997) 843.

28. M. ES-SOUNI, A. BARTERLS and R. WAGNER, "Structural Intermetallics," edited by R. Darolia, J. J. Lewandoski, C. T. Liu, P. L. Martin, D. B. Miracle and M. V. Nathal (The Minerals, Meals & Materials Society, 1993) p. 335.
29. T. TAKAHASHI and H. OIKAWA, in "High-Temperature Ordered Intermetallic Alloys IV," edited by. L. A. Johnson, D. P. Pope and J. O. Stiegler (Materials Research Society, Pittsburgh, Pa, 1991) p. 721.
30. P. L. MARTIN, M. G. MENDIRATTA and H. A. LIPSITT, *Metall. Trans.* **A14** (1983) 2170.
31. D. A. WHEELER, B. LONDON and D. E. LARSEN, JR., *Scripta Metall. et Mater.* **26** (1992) 939.
32. J. S. HUANG and Y. W. KIM, *ibid.* **25** (1991) 1901.
33. H. OIKAWA, *Mater. Sci. Eng.* **A153** (1992) 427.
34. S. KROLL, H. MEHRE, N. STROWIJK, C. HERSIG, R. ROSENKRANZ and G. FROMMERYER, *S. Metallkd.* **83** (1992) 8.

Received 11 February
and accepted 15 November 2000